

13. COPPER-RICH SULFIDE DEPOSIT NEAR 23°N, MID-ATLANTIC RIDGE: CHEMICAL COMPOSITION, MINERAL CHEMISTRY, AND SULFUR ISOTOPES¹

Katsuo Kase,² Masahiro Yamamoto,² and Tsugio Shibata²

ABSTRACT

In Snake Pit massive sulfide fragments and friable, unconsolidated material recovered during ODP Leg 106, isocubanite and pyrite are generally the predominant phases, followed by marcasite, chalcopyrite, sphalerite, and pyrrhotite. Detailed analyses of paragenetic relations of minerals indicate that isocubanite first precipitated together with pyrrhotite. With decreasing temperature, chalcopyrite and sphalerite precipitated, and at the latest stage colloform sphalerite-pyrite (or colloform marcasite) formed. Isocubanite usually has exsolution lamellae of chalcopyrite and less commonly of pyrrhotite.

The average bulk chemical composition of the friable, unconsolidated material indicates that it is rich in copper, reflecting the dominance of isocubanite in the specimens, and is characterized by high Co, low Pb, and Ag contents. Sulfur isotope ratios are very uniform, ranging in $\delta^{34}\text{S}$ from +1.2 to +2.8‰. The obtained values are apparently low, compared to those for the eastern Pacific sulfide samples, reflecting a smaller contribution of seawater sulfate in the Snake Pit sulfide deposit.

INTRODUCTION

During ODP Leg 106, an active high-temperature vent field was discovered on the Mid-Atlantic Ridge (MAR) rift valley near 23°22'N, 44°57'W. The active vent field named the Snake Pit hydrothermal area is located on a small terrace near the crest of the median ridge about 25 km south of the Kane Fracture Zone at the water depth of 3530 m (Fig. 1). Preliminary results obtained during ODP Leg 106 on the geology and mineralogy of hydrothermal deposits in the Snake Pit area have been reported by Detrick et al. (1986).

The vent field occupies a large area (>40,000 m²) and consists of numerous mounds and chimneys (up to 11 m high). Most of the chimneys appeared to be inactive, but plumes of black smoke were observed rising from the top and sides of a large chimney. The temperature of hydrothermal solutions emanating from this large black smoker vent was found to be 350°C in the submersible study subsequently conducted by *Alvin* in May 1986 (Sulanowska et al., 1986).

Ten shallow holes (649A through -J) were drilled in the Snake Pit area. Holes 649A through -G were located near the large, active chimney found in the middle of the hydrothermal field (Fig. 2). The other three holes (649H, -I, and -J) were drilled about 65–70 m west of the large, active vent. Drilling was terminated in basaltic basement in most cases. Recovery rates were disappointingly low, ranging from zero to a few percent, except in Hole 649B, where an almost complete section was obtained through the hydrothermal deposit. The cores of Hole 649B are, however, badly disturbed and consist of friable, unconsolidated material which gradually coarsens downward. The grain size of this material ranges from fine-grained sands to angular, massive cut fragments up to few centimeters in length. Hole 649G also recovered brassy massive sulfides from an extremely hard horizon about 8.5 m below the seafloor. In this paper, we describe the mineralogy, bulk chemistry, and sulfur isotopes of the specimens obtained

from the Snake Pit sulfide deposit and examine its depositional conditions.

ANALYTICAL PROCEDURES

Data acquisition for this study consisted of ore microscopy, microprobe analyses, bulk major and trace element analyses, and sulfur isotope analyses. Microprobe analyses of sulfide minerals were carried out on a three-channeled JEOL X-ray microprobe analyzer operated at 25 kV and 0.01–0.02 μA sample currents. The correction procedure was that of Sweatman and Long (1969).

For the determinations of sulfur isotope ratios, sulfide samples were converted into BaSO_4 , which was thermally decomposed to SO_2 (Yanagisawa and Sakai, 1983). The isotope analysis was made with a Hitachi RMU-6RS mass spectrometer. The results of isotope analysis are given in $\delta^{34}\text{S}$ value (‰) relative to the Canyon Diablo troilite. The precision is better than $\pm 0.2\text{‰}$.

The sulfide samples were decomposed by a mixture of HNO_3 and HBr for bulk chemical analysis of sulfide fractions. The residues in the treatment were mostly irregular-shaped silica and iron oxide. Major metals (Fe, Cu, and Zn) were analyzed by EDTA titration and sulfur was determined gravimetrically as BaSO_4 . Minor elements (Co, Ni, Cd, Mn, Pb, and Ag) were determined by atomic absorption spectrometry and Se by spectrophotometry using *o*-phenylenediamine as a color reagent (Ariyoshi et al., 1960).

MINERAL PARAGENESIS AND ORE TEXTURES

We received 11 massive sulfide specimens (i.e., 9 fragments from Hole 649B and 2 slices cut from the massive specimen of Hole 649G) and 5 vials of the friable, unconsolidated material from Hole 649B for our detailed onshore study. Isocubanite and pyrite are generally the predominant phases in the Snake Pit sulfide specimens, followed by marcasite, chalcopyrite, and sphalerite with lesser amounts of pyrrhotite, covellite, an alteration phase derived from pyrrhotite, and Fe-hydroxide. Amorphous silica is abundant in some samples. A jordanite-like mineral occurs rarely as fine bands in colloform sphalerite. Wurtzite and sulfate minerals such as anhydrite and barite were not detected in our samples, consistent with the results by Detrick et al. (1986). According to Sulanowska et al. (1986), however, anhydrite is very common in samples taken from the same area by the submersible *Alvin*, especially in the upper parts of taller chimneys. Talc and chlorite, which are described by Detrick et al. (1986) to accompany sulfides in minor amounts, could not be positively identified in the present samples.

¹ Detrick, R., Honnorez, J., Bryan, W. B., Juteau, T., et al., 1990. *Proc. ODP, Sci. Results*, 106/109: College Station, TX (Ocean Drilling Program).

² Department of Earth Sciences, Okayama University, Tsushima, Okayama 700, Japan.

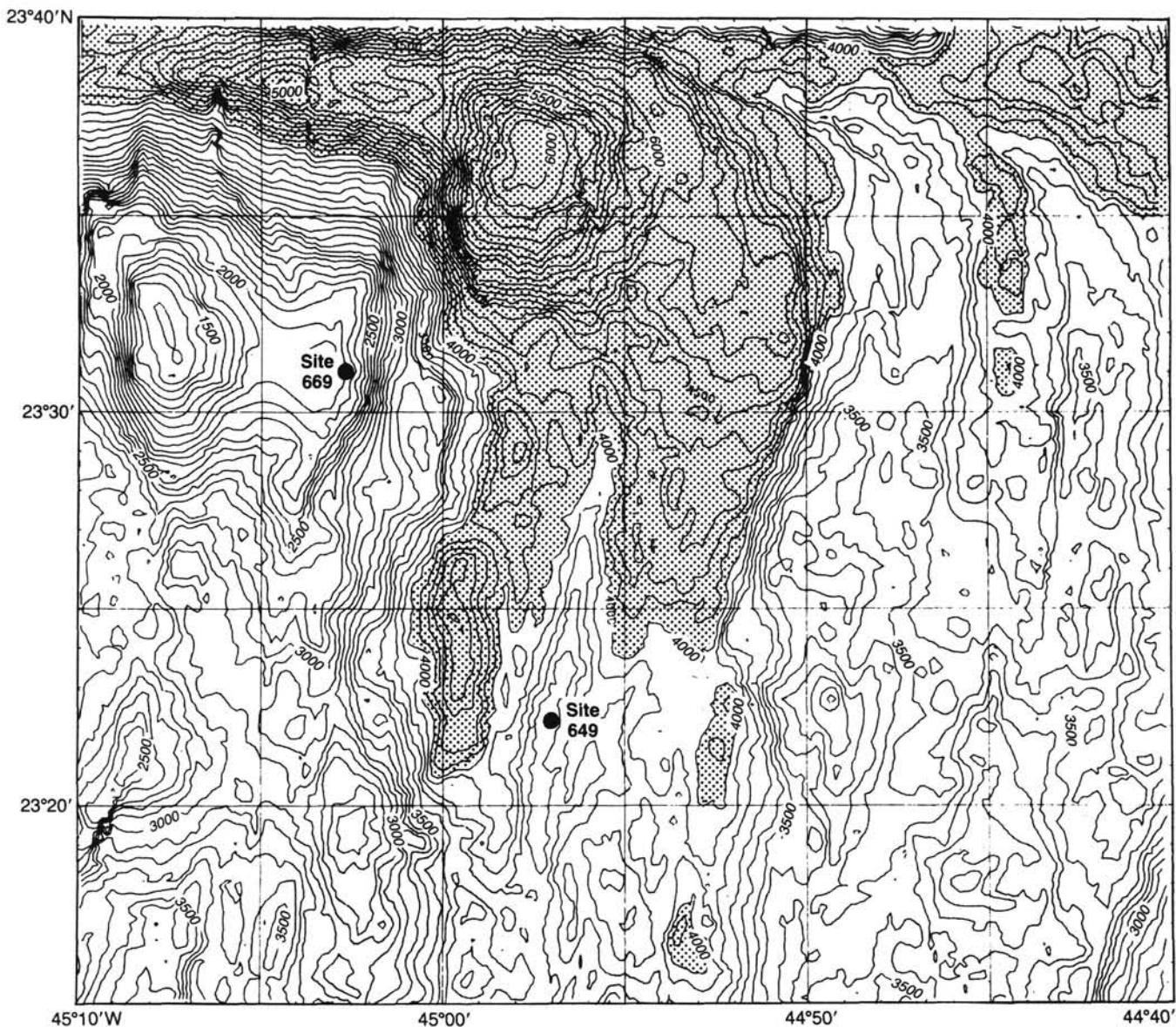


Figure 1. SeaBeam bathymetry of the region at the Mid-Atlantic Ridge 23°30'N (Pockalny et al., 1985) and location of the Snake Pit hydrothermal area (Site 649). Contour interval is 100 m; shading indicates depths greater than 4000 m.

Most of the fine- to coarse-grained, unconsolidated material from Hole 649B is black in hand specimen. The larger, angular sulfide fragments (0.7–2.5 cm in length) from Hole 649B and the massive sulfide specimens from Hole 649G show a variety of colors reflecting differences in modal proportions of the major constituent minerals; i.e., isocubanite, chalcopyrite, and sphalerite. Mainly based on the observed colors in hand specimen, we classified the 11 massive sulfide specimens into three groups: (1) brassy yellow fragments, (2) yellow fragments, and (3) dark gray fragments and, in what follows, we describe the paragenesis and texture of the massive sulfide specimens as well as the friable, unconsolidated sulfide specimens accordingly. Brief sample descriptions are given in Table 1.

Brassy yellow massive sulfide fragments

The brassy yellow specimens (two chips from Hole 649G and four fragments from Hole 649B) are composed dominantly of isocubanite. The two specimens from Hole 649G consist of

spherical isocubanite grains (0.1–0.3 mm in diameter), and the four specimens from Hole 649B consist of mosaic aggregates of isocubanite grains (<1 mm). The isocubanite grains from both holes almost invariably contain exsolution lamellae of chalcopyrite. Abundances of chalcopyrite lamellae and the exsolution textures in the isocubanite grains are similar to one another within each, single specimen, but vary considerably from specimen to specimen.

The coarsely crystalline isocubanite grains of two massive sulfide specimens (649B-1D-8D, 90–120 cm(a) and 649B-1D-8E, 120–150 cm(a)) contain only small amounts of chalcopyrite lamellae. Some grains appear to be free from exsolution lamellae under the reflected microscope. Back-scattered electron images, however, reveal that even some of these optically homogeneous isocubanite grains include abundant cryptocrystalline exsolution bodies about 0.5 μm in diameter (Plate 2-1). Chalcopyrite lamellae frequently form a rectangular, lattice-like exsolution texture, which indicates that chalcopyrite has exsolved along (100) of the host isocu-

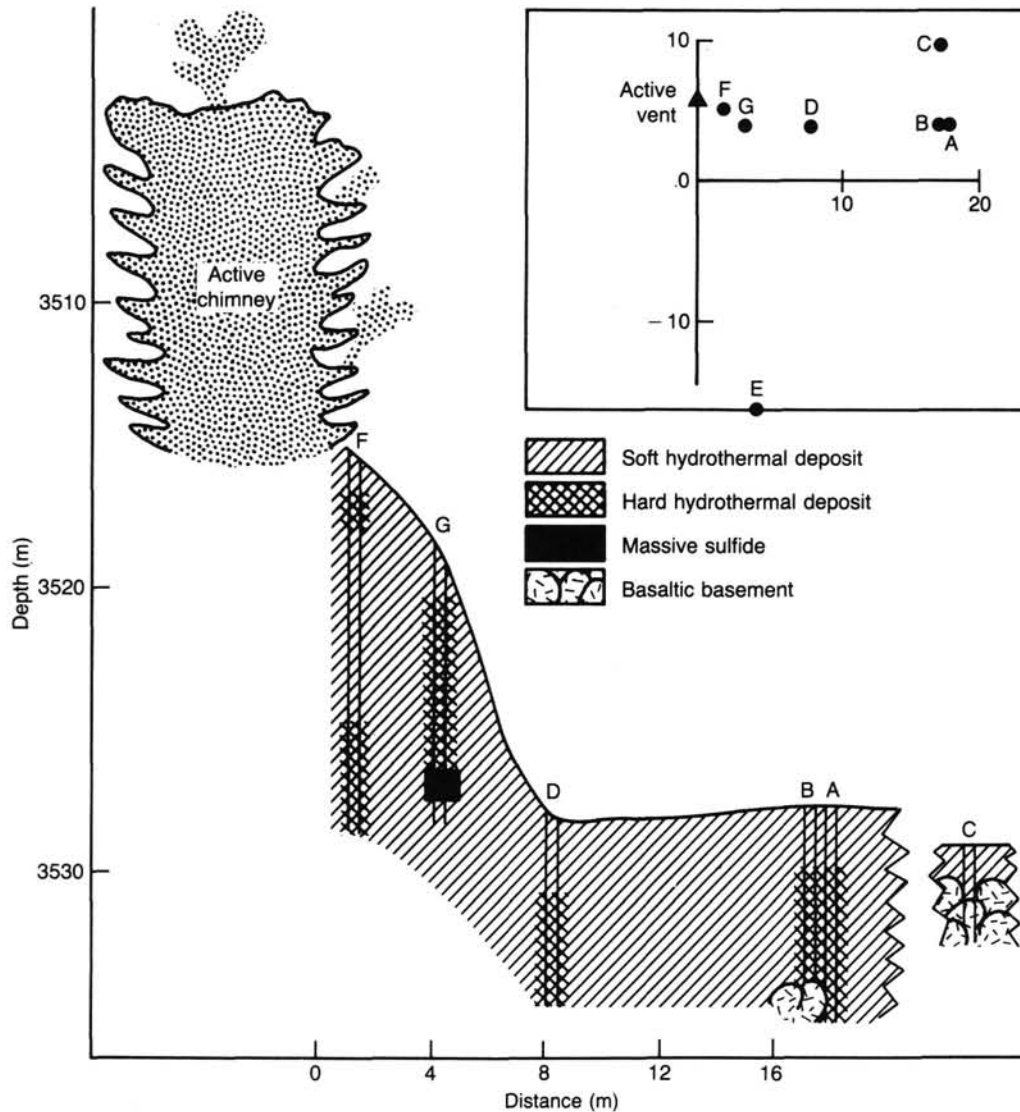


Figure 2. Cross section of the Snake Pit hydrothermal deposit near the large black smoker, showing the drilling result at Site 649. Inset shows position of drill holes relative to the large smoker.

banite (Plate 2-2 and -3). Another phase with thin lenticular form exsolves in the direction diagonal to the rectangular chalcopyrite lattice (Plate 2-2). The back-scattered electron images and semi-quantitative analyses suggest that this phase probably has a Cu/Fe ratio intermediate between the chalcopyrite lamella and host isocubanite.

The spherical isocubanite grains from Hole 649G are nearly always rimmed by chalcopyrite about 0.005–0.05 mm thick. These isocubanites with the chalcopyrite rim coexist with Fe-sulfides such as marcasite, pyrite, and pyrrhotite. Pyrrhotite fills the interstices between isocubanite grains, whereas most of the Fe-disulfides with irregular outlines occur between isocubanite grains, suggesting that they have replaced isocubanite. Euhedral, cubic pyrite crystals are sometimes enclosed in isocubanite grains (Plate 1-1).

Pyrrhotite occurs usually as long prismatic crystals (<0.5 mm in length) in the coarse-grained massive sulfide specimens (Plate 1-2). The pyrrhotite crystals are commonly replaced by marcasite or altered to an unidentified sulfide phase with low reflectivity and moderate anisotropy. Pyrrhotite crystals with granular and short prismatic forms occur also in the cores of

isocubanite, suggesting that the pyrrhotite acted as a seed on which isocubanite grew. In the two massive sulfide specimens where only small amounts of chalcopyrite have exsolved from isocubanite, tiny grains with lenticular or irregular outlines of pyrrhotite are also enclosed in isocubanite grains (Plate 1-3). This type of pyrrhotite may be an exsolution product from isocubanite.

A few small grains of sphalerite are contained in the brassy yellow massive sulfide fragments. In one sample from Hole 649G, sphalerite is enclosed in an isocubanite grain with shrinkage cracks, and this isocubanite grain is in turn surrounded by pyrite (Plate 1-4). Like chalcopyrite blebs in sphalerites of on-land sulfide deposits, blebs of isocubanite are observed in some of the Snake Pit sphalerite grains. No discrete grains of chalcopyrite are observed in the brassy yellow massive sulfide fragments.

Yellow massive sulfide fragments

Specimen 649B-1D-8E, 120–150 cm(c) is composed mainly of chalcopyrite with considerable amounts of sphalerite. Another yellow fragment (649B-1D-8E, 120–150 cm(d)) consists

Table 1. Brief descriptions of analyzed samples.

Sample no. (interval in cm)	Type ^a	Constituent minerals ^b
649B-1D-8D 90–120(a)	Brassy yellow massive fragment	icb sp cp po
649B-1D-8D 90–120(b)	Brassy yellow massive fragment	icb sp cp po mc uk
649B-1D-8D 90–120(c)	Yellow massive fragment	cp icb
649B-1D-8D 90–120(d)	Dark brassy yellow massive fragment with a dark gray band	Brassy yellow portion: mc icb py po sp; gray band: sp icb mc py po uk
649B-1D-8E 120–150(a)	Brassy yellow massive fragment	icb sp cp po py mc
649B-1D-8E 120–150(b)	Brassy yellow massive fragment	icb cp py mc sp uk
649B-1D-8E 120–150(c)	Yellow massive fragment	cp sp py icb
649B-1D-8E 120–150(d)	Yellow massive fragment	cp sp py icb cov
649B-1D-8E 120–150(e)	Dark gray massive fragment	sp mc icb py cp po uk
649G-1D-1, 2	Brassy yellow fragment	icb cp py mc sp po
649G-1D-1 14–16, #4	Brassy yellow fragment	icb cp py po mc
649B-1D-2 14–20	Unconsolidated material (0.1–0.3 mm)	icb cp py mc sp po Fe-ox uk cov
649B-1D-5 80–86	Unconsolidated material (0.1–0.3 mm)	icb cp py mc sp po Fe-ox uk cov
649B-1D-7 84–90	Unconsolidated material (<1 mm)	icb cp py mc sp po Fe-ox uk cov
649B-1D-8 50–56	Unconsolidated material (<1 mm)	icb cp py mc sp po Fe-ox uk cov jor
649B-1D-8 134–140	Unconsolidated material (<1 mm)	icb cp py mc sp po Fe-ox uk cov

^a Numbers in parentheses give ranges for grain size.

^b Abbreviations for minerals are as follows: icb = isocubanite; sp = sphalerite; cp = chalcopyrite; py = pyrite; po = pyrrhotite; mc = marcasite; cov = covellite; uk = an unidentified phase derived through alteration of pyrrhotite; Fe-ox = Fe hydroxide; and jor = jordanite.

mainly of chalcopyrite with lesser amounts of sphalerite, pyrite, and marcasite. Covellite occurs as an alteration product of chalcopyrite along its grain margins in this specimen. Interlocking coarsely-crystalline chalcopyrite grains are found in the above two sulfide specimens. Chalcopyrite in these specimens very rarely contains fine lamellae of isocubanite. A noteworthy feature is that sphalerite is much more abundant in these specimens than in the isocubanite-dominant massive fragments.

Specimen 649B-1D-8D, 90–120 cm(c) comprises nearly equal amounts of chalcopyrite and isocubanite with no other sulfide mineral. The modal proportions of chalcopyrite and isocubanite, however, vary significantly from domain to domain in the specimen. The ore texture of the isocubanite-rich domains are similar to that of the brassy yellow fragments, and the same texture as that of the isocubanite-rich domains is often seen at the centers of chalcopyrite grains in the chalcopyrite-rich domains (Plate 1-5).

Dark gray sulfide fragments

In Specimen 649B-1D-8E, 120–150 cm(e), spherical, colloform marcasite grains with a sphalerite overgrowth are cemented with interstitial amorphous silica (Plate 1-6). Short, prismatic pyrrhotite is seen at the center of some marcasite spheres. No blebs of chalcopyrite or isocubanite could be detected in the sphalerite overgrown on the spherical marcasite. In small portions of the same specimen, various separate as well as composite mineral grains are also cemented with amorphous silica; they include isocubanite, sphalerite, chalcopyrite, pyrrhotite, marcasite, and pyrite. Some of these

grains are angular, broken fragments, and hence it is inferred that this specimen represents cemented sulfide debris containing grains from various stages of mineralization.

A 7–8-mm-thick, dark gray band occurs in the dark brassy yellow massive sulfide specimen (649B-1D-8D, 90–120 cm(d)). This dark gray band is composed mainly of sphalerite grains having abundant isocubanite with lesser amounts of pyrrhotite and pyrite in the cores. Blebs of isocubanite are common in this sphalerite. The sphalerite occasionally develops hexagonal habits, and such sphalerite commonly displays well-developed sector-zoning (Plate 2-5). Although its crystal habit suggests that this sphalerite might have originally precipitated as wurtzite, X-ray diffraction shows that it is now not wurtzite but sphalerite. The sphalerite is partially penetrated by dendritic marcasite and pyrite. Discrete chalcopyrite grains do not occur in the sphalerite-rich bands.

Friable, unconsolidated material

The friable, unconsolidated material consists of various kinds of sulfide grains, which include isocubanite with or without chalcopyrite exsolution lamellae, chalcopyrite, sphalerite accompanying isocubanite in its core or as bands, colloform sphalerite-pyrite (or marcasite), colloform pyrite, and partially or completely altered pyrrhotite. In addition, Fe-hydroxide, which probably derived from sulfides through oxidation, is also commonly found in these specimens. All of these minerals occur as discrete grains or aggregates of smaller grains. A few are broken fragments.

The observed mineral constituents are essentially identical between the coarse- and fine-grained materials. As described in the previous sections, most of these minerals are also found in the massive sulfide fragments. The friable, unconsolidated sulfide specimens are, however, different from the massive sulfide specimens in that in the former specimens, we observe growth bands of a jordanite-like mineral in sphalerite (Plate 1-7), colloform pyrite, zoned grains in which chalcopyrite, isocubanite, and sphalerite precipitated in this sequence from the core to rim (Plate 1-8), and Fe-hydroxide. Isocubanite grains without chalcopyrite exsolution lamellae are more frequently observed in the friable, unconsolidated material.

BULK CHEMISTRY

Partial, bulk chemical analyses of five friable, unconsolidated specimens and one massive specimen from the Snake Pit hydrothermal deposit are presented in Table 2. The massive sulfide specimen is composed of aggregates of spherical isocubanite with chalcopyrite rims. In order to assess chemical characteristics of the Snake Pit sulfide deposit, we list in Table 3 the bulk chemical data reported previously for sulfide-rich specimens from the East Pacific Rise (EPR) at 21°N and the Galapagos Spreading Center (GSC) (Bischoff et al., 1983).

There is no significant difference in major and trace element abundances or sulfur-metal ratios among the five friable, unconsolidated sulfide specimens. As the cores of Hole 649B were disturbed during the drilling, it is unclear whether the compositions of these five specimens are indicative of the respective horizons from which they were sampled. The bulk chemical data of these specimens have been averaged to obtain a bulk composition of the basal mound deposit at this location (No. 1 in Table 3). The massive sulfide fragment is rich in copper and its bulk composition is consistent with the isocubanite-dominant mineralogy. The amounts of insoluble silicate fractions in the HBr-HNO₃ solution are much smaller for the massive sulfide fragment than for the friable, unconsolidated sulfide specimens (Table 2).

The bulk chemical analyses of the Snake Pit sulfide specimens indicate the following characteristics: (1) they are more

Table 2. Bulk analyses of polymetallic sulfide samples from the Snake Pit hydrothermal deposit.

Sample no.	649B-1D-2 14-20	649B-1D-5 80-86	649B-1D-7 84-90	649B-1D-8 50-56	649B-1D-8 134-140	649G-1D-1 14-16, #4
Weight percent						
Cu	5.39	5.50	6.07	7.15	5.68	16.08
Zn	1.88	2.22	2.81	1.92	2.55	0.12
Fe	36.14	37.67	36.07	38.87	38.23	44.85
S	31.34	33.57	32.89	34.11	35.44	36.10
Total	74.75	78.96	77.84	82.05	81.90	97.15
Parts per million						
Ag	20	20	20	20	10	<10
Pb	400	350	330	350	340	30
Cd	230	240	310	195	300	50
Co	640	560	780	600	510	730
Ni	<10	<10	<10	<10	<10	<10
Mn	110	140	120	110	180	20
Se	267	263	266	351	249	n.d.
Atomic ratio						
S/Σ metal	1.28	1.32	1.31	1.27	1.36	1.06

Table 3. Comparison of the average Snake Pit sulfide with other submarine sulfide analyses.

	Snake Pit ^a	EPR 21°N ^b	GSC ^c
(wt%)			
Cu	5.96	0.81	4.98
Zn	2.28	32.3	0.14
Pb	0.035	0.32	<0.07
Fe	37.40	19.2	44.1
S	33.47	35.3	52.2
(ppm)			
Ag	18	159	10
Cd	255	600	32
Co	618	<3.5	482
Ni	<10	3	3
Mn	132	390	140
Se	280	63	

^a Average of five friable, unconsolidated sulfide samples from the Snake Pit hydrothermal deposit (the present study).

^b Average of three inactive basal mound sulfides from the EPR at 21°N (Bischoff et al., 1983).

^c Brassy, coarsely crystalline massive sulfide from Galapagos Spreading Center (Bischoff et al., 1983).

enriched in copper than in zinc, (2) in general, their lead and silver contents are low, and (3) cobalt is present in significant amounts. The chemical characteristics observed in the friable, unconsolidated material of the Snake Pit deposit are basically identical with those of the coarsely crystalline massive sulfide specimen from the GSC, but are remarkably different from those of the mound sulfide specimens from the EPR at 21°N, especially in terms of Cu and Zn contents (Table 3). Some of the Zn-rich sulfides from the EPR at 21°N have high levels of lead and silver. Most of the Zn-rich sulfides known so far from the eastern Pacific (e.g., those from the Juan de Fuca Ridge and the Guaymas Basin) have chemical characteristics similar to those of the EPR at 21°N (Bischoff et al., 1983; Davis et al., 1987; Hannington et al., 1986; Koski et al., 1984).

SULFUR ISOTOPES

Sulfur isotope ratios were measured for eight massive sulfide fragments and the five friable, unconsolidated sulfide specimens. From the brassy yellow massive sulfide specimen

Table 4. Sulfur isotope ratios of sulfide specimens. Abbreviations for minerals are the same as in Table 1.

Sample no.	Major minerals	δ ³⁴ S (‰)
1. Massive sulfide specimens		
649B-1D-8D, 90-120(a)	icb	+1.2
649B-1D-8D, 90-120(b)	icb	+2.7
649B-1D-8D, 90-120(d) ^a	mc icb py	+1.5
649B-1D-8D, 90-120(d) ^b	sp icb mc	+2.3
649B-1D-8E, 120-150(b)	icb	+1.7
649B-1D-8E, 120-150(d)	cp	+2.6
649B-1D-8E, 120-150(e)	sp mc icb py cp	+1.8
649G-1D-1, 14-16, #4	icb cp	+2.5
649G-1D-1, 2	icb cp py	+2.8
2. Friable, unconsolidated sulfide specimens		
649B-1D-2, 14-20	icb cp py mc sp	+1.4
649B-1D-5, 80-86	icb cp py mc sp	+1.9
649B-1D-7, 84-90	icb cp py mc sp	+2.0
649B-1D-8, 50-56	icb cp py mc sp	+1.8
649B-1D-8, 134-140	icb cp py mc sp	+2.2

^a Brassy yellow portion.

^b Sphalerite-rich band.

with a sphalerite-rich band (649B-1D-8D, 90-120 cm(d)), two samples were taken: one from the band and the other from the brassy yellow portion. The results are given in Table 4, together with the major constituent minerals.

The δ³⁴S values of the massive sulfide fragments are +1.2 to +2.8‰. The mineral assemblage and modal proportion of constituent sulfide minerals are widely variable from specimen to specimen, but do not clearly correlate with the δ³⁴S values. The δ³⁴S values of the friable, unconsolidated sulfide specimens are +1.4 to +2.2‰, and all fall within the range for the massive sulfide specimens. The more homogeneous distribution of δ³⁴S values for the friable, unconsolidated specimens seems to be natural because they have virtually the same mineralogy and bulk chemistry. The overall mean of the 14 measured isotope ratios is +2.03 ± 0.50 (1σ). Sulfur isotope studies of the eastern Pacific deposits have shown that the δ³⁴S values of sulfide samples from the EPR at 21°N are in the range from +0.7‰ to +4.5‰ with a mean of +2.5 (Hekinian et al., 1980; Arnold and Sheppard, 1981; Styrts et al., 1981; Kerridge et al., 1983; Zierenberg et al., 1984). The δ³⁴S values for sulfide samples from the Juan de Fuca Ridge are in the range +1.4‰ to +5.7‰ with a mean of +3.1‰ (Shanks et al., 1984; Shanks and Seyfried, 1987) and from the GSC are +5.4

to +6.3‰ (Skirrow and Coleman, 1982). Compared to the eastern Pacific deposits cited above, the $\delta^{34}\text{S}$ values of the Snake Pit sulfide specimens are apparently low as all are within the lower half of the overall range of the eastern Pacific sulfide samples.

MINERAL CHEMISTRY

Isocubanite

The broadness and abundance of chalcopyrite lamellae in isocubanite vary significantly from specimen to specimen, and in the case of the friable, unconsolidated material, these vary even from grain to grain within a single specimen. On the basis of exsolved phases present and their relative amounts, isocubanite grains found in the massive sulfide fragments are classified into three groups: (1) isocubanite grains with small amounts of exsolved chalcopyrite and pyrrhotite, (2) isocubanite grains with small to moderate amounts of exsolved chalcopyrite but with no pyrrhotite lamellae, and (3) isocubanite grains with large amounts of chalcopyrite lamellae but also with no pyrrhotite lamellae. A variety of isocubanite grains are found in the friable, unconsolidated material and they, in addition to the above three groups, include those with no exsolution phases.

Representative compositions of isocubanite are listed in Table 5. Some of the microprobe analyses were obtained for the homogeneous domains of isocubanite alone with a focused electron beam (2–3 μm in diameter), but others are bulk chemical compositions for isocubanite plus exsolved phases and were obtained by averaging 10–20 spot analyses made with a defocused beam (30 μm). The chemical compositions of isocubanite are plotted with different symbols for each of the three isocubanite groups in Figure 3A, -B, and -C. Isocubanite grains from the friable, unconsolidated material are plotted in a separate diagram (Fig. 3D) and are listed under Group 4 in Table 5. Also shown in Figure 3 are compositional fields of

solid solutions determined experimentally at 350°C in the system Cu-Fe-S (Sugaki et al., 1975).

As shown in Fig. 3A, the first group isocubanites are plotted at or very close to the composition $\text{Cu}_{15.3}\text{Fe}_{34.9}\text{Zn}_{0.1}\text{S}_{49.7}$ with the most Fe-rich composition being $\text{Cu}_{14.9}\text{Fe}_{35.4}\text{Zn}_{0.1}\text{S}_{49.6}$ (No. 1 in Table 5). The bulk compositions for isocubanite plus chalcopyrite lamellae are only slightly poorer in Fe than the compositions for the homogeneous domain of isocubanite alone. The compositional range for this group of isocubanite is displaced significantly toward the (Fe + Zn + Co) -S side of the ternary diagram compared to that of the intermediate solid solution (iss) in the system Cu-Fe-S determined experimentally at 350°C by Sugaki et al. (1975).

The second group of isocubanite has a wider compositional range than the first, extending toward the stoichiometric composition of cubanite (Fig. 3B). Specimen 649B-1-8D, 90–120 cm(b) contains lath-shaped pyrrhotite. The isocubanite in this specimen is relatively rich in Fe, ranging from 34.32 to 34.75 atomic% (No. 3 in Table 5), and in this respect, is not different from the first group of isocubanite. The isocubanite is generally poor in Fe in the other two massive specimens, in which pyrrhotite is absent (No. 4 in Table 5).

The third group isocubanite grains from Specimen 649G-1D-1, 14–16 cm, #4 include pyrrhotite in their cores. The bulk compositions for such isocubanite plus chalcopyrite lamellae in this specimen are concentrated in a small field near the stoichiometric composition of cubanite (b in Fig. 3C and No. 6 in Table 5). Slightly bright domains are detected in the back-scattered electron images of this isocubanite (2 in Plate 2-4). Such bright domains are free of chalcopyrite exsolution lamellae, but are rich in Cu compared with the bulk composition (an open circle marked with a 2 in Fig. 3C and No. 7 in Table 5). These bright domains might represent an intermediate stage toward the formation of chalcopyrite lamellae during an exsolution process. The dark, homogeneous domain of the same isocubanite has an Fe-rich com-

Table 5. Representative microprobe analyses of isocubanite.

Analysis no. ^a	Group 1		Group 2			Group 3			Group 4		
	1	2	3	4	5	6	7	8	9	10	11
(wt%)											
Cu	20.96	21.37	21.31	22.25	21.42	23.74	27.19	21.77	25.63	25.03	21.12
Fe	43.73	42.89	42.71	41.50	41.71	40.85	38.22	42.79	39.34	39.91	42.87
Zn	0.12	0.28	0.15	0.22	1.82	0.10	0.06	0.09	0.18	0.10	0.86
Co	n.d.	0.02	0.18	0.31	0.13	0.06	0.06	0.11	0.12	0.11	0.34
S	35.21	34.96	35.12	35.27	35.17	35.40	34.89	35.12	35.20	35.35	35.34
Total	100.02	99.52	99.47	99.55	100.25	100.15	100.42	99.88	100.47	100.50	100.53
(atomic%)											
Cu	14.91	15.29	15.24	15.90	15.24	16.89	19.43	15.52	18.25	17.79	14.96
Fe	35.39	34.92	34.75	33.75	33.78	33.07	31.08	34.71	31.97	32.28	34.56
Zn	0.09	0.19	0.10	0.15	1.26	0.07	0.04	0.06	0.12	0.07	0.59
Co	—	0.02	0.14	0.24	0.10	0.05	0.05	0.09	0.10	0.08	0.26
S	49.61	49.58	49.77	49.96	49.62	49.92	49.40	49.62	49.66	49.78	49.63

^a Analysis numbers designate the following samples:

1. Homogeneous domain of isocubanite, 649B-1D-8E, 120–150 cm(a).
2. Bulk analysis for an isocubanite grain with thin chalcopyrite lamellae, 649B-1D-8D, 90–120 cm(a).
3. Bulk analysis for an isocubanite grain with a minor amount of chalcopyrite lamellae, 649B-1D-8D, 90–120 cm(b).
4. Homogeneous isocubanite grain without exsolved lamellae, 649B-1D-8D, 90–120 cm(c).
5. Bulk analysis for an isocubanite grain with cryptocrystalline, minute exsolved phase (0.1 μm in diameter), 649G-1D-1, 2 cm.
6. Bulk analysis for an isocubanite grain with a moderate amount of chalcopyrite lamellae, 649G-1D-1, 14–16 cm, #4.
7. Light-gray domain in back-scattered electron image, the same isocubanite grain as Analyses 6 and 8.
8. Dark domain in back-scattered electron image, the same isocubanite grain as Analyses 6 and 7.
9. Bulk analysis for an isocubanite grain with a large amount of chalcopyrite lamellae, 649B-1D-8E, 120–150 cm(b).
10. Homogeneous, small isocubanite grain without exsolved lamellae, 649B-1D-8, 50–56 cm.
11. Bulk analysis for isocubanite plus thin chalcopyrite lamellae of the composite grain zoned concentrically from chalcopyrite at the core through isocubanite to sphalerite at the rim, 649B-1D-8, 50–56 cm.

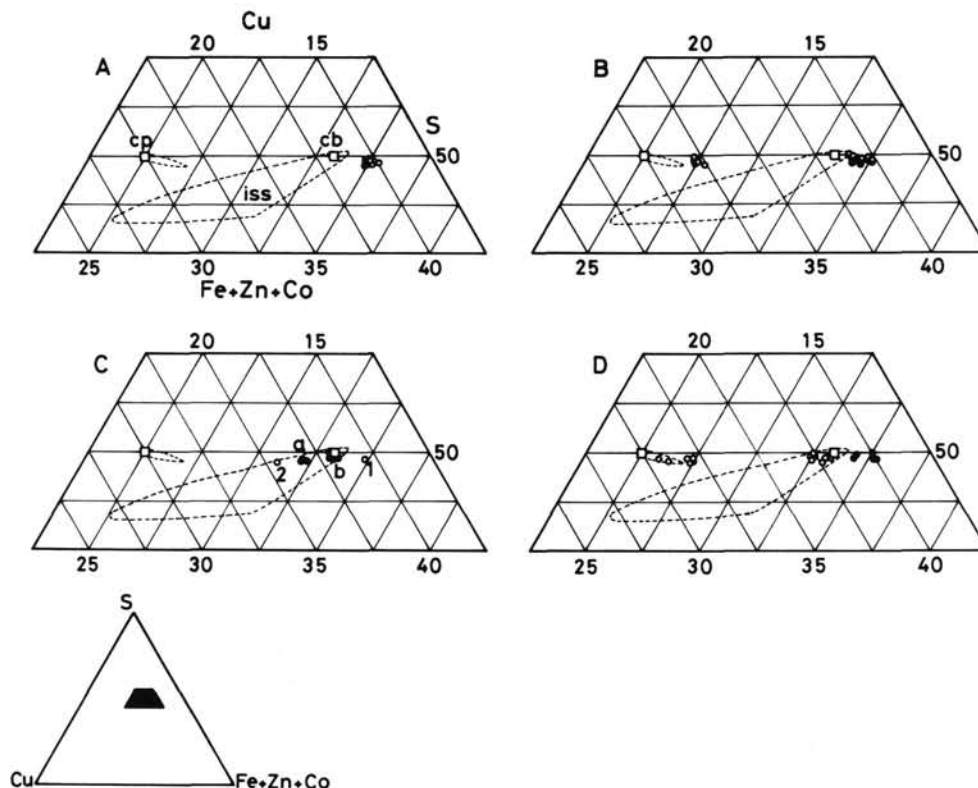


Figure 3. Microprobe analyses of isocubanite and chalcopyrite plotted in a portion of the system Cu-(Fe + Zn + Co)-S. Open circles indicate compositions obtained for the homogeneous domains of isocubanite and chalcopyrite; solid circles indicate bulk compositions obtained for isocubanite host plus chalcopyrite lamellae; and open squares indicate stoichiometric compositions for chalcopyrite (cp) and cubanite (cb). Broken lines indicate the compositional fields for iss and chalcopyrite solid solution at 350°C (Sugaki et al., 1975). A. Group 1 isocubanite compositions. B. Group 2 isocubanite compositions. C. Group 3 isocubanite compositions. The compositions marked with a and b are from Samples 649B-1D-8E, 120–150 cm(b) and 649G-1D-1, 14–16 cm, #4, respectively. The compositions marked with 1 and 2 represent those of dark and bright domains of isocubanite on the back-scattered electron image, respectively (Sample 649G-1D-1, 14–16 cm, #4). D. Isocubanite (Group 4) and chalcopyrites with various modes of occurrence from the friable, unconsolidated material (Sample 649B-1D-8, 50–56 cm).

position (No. 8 in Table 5) that is plotted outside of the experimentally determined compositional field for iss in Figure 3C. The bulk compositions for isocubanite from Specimen 649B-1D-8E, 120–150 cm(b) (Plate 2-3) are indicated by solid circles marked with an a in Figure 3C, and a representative analysis is listed in Table 5 (No. 9). This isocubanite does not coexist with pyrrhotite.

The homogeneous isocubanite with no chalcopyrite lamellae in the friable, unconsolidated material is relatively rich in Cu as shown by open circles in Figure 3D (No. 10 in Table 5) and is similar in composition to the bulk compositions of the third group of isocubanite.

The Snake Pit isocubanite contains small quantities of Zn and Co, up to 1.26 and 0.26 atomic%, respectively. The Co-bearing isocubanite must be mainly responsible for the high Co contents of the bulk sample analyses as noted previously. The maximum Zn content in isocubanite enclosing sphalerite, with many but tiny isocubanite blebs (Plate 1-4), is very close to 1.2 atomic%—the maximum solubility of Zn in iss at 300°C and 500 kg/cm² determined experimentally by Kojima and Sugaki (1985). The back-scattered electron images revealed that no Zn-rich phase is included in this isocubanite grain. So, it is likely that Zn is in solid solution. The Zn

Table 6. X-ray powder data of isocubanite.

hkl	1			2		
	I/I ₀	d _{obs}	d _{calc}	I/I ₀	d _{obs}	d _{calc}
111	10	3.059	3.062	10	3.062	3.061
200	2	2.647	2.652	1	2.650	2.651
220	7	1.876	1.875	4	1.875	1.875
311	5	1.602	1.599	2	1.598	1.599
400	2	1.327	1.326	1	1.326	1.326
331	—	—	—	1	1.216	1.216
		a = 5.303 Å			a = 5.302 Å	

1. From the EPR 21°N (Caye et al., 1988).

2. Sample 649B-1D-8E, 120–150 cm(a) from the Snake Pit hydrothermal area, MAR at 23°N (the present study).

contents of most isocubanite are, however, usually less than 0.3 atomic%, and sphalerite occurs only sporadically in the isocubanite-dominant massive sulfide specimens.

X-ray reflections from powder diffraction data were indexed in terms of a face-centered cubic lattice with a cell edge of 5.302 Å (Table 6). The cell edge of the Snake Pit isocubanite is almost identical to that of the isocubanite from the EPR 21°N (Caye et al., 1988).

Table 7. Representative microprobe analyses of chalcopyrite.

Analysis no. ^a	1	2	3
(wt%)			
Cu	31.42	33.62	33.54
Fe	33.97	31.97	32.15
Zn	0.06	0.16	0.00
Co	0.06	n.d.	0.01
S	34.80	34.61	34.76
Total	100.31	100.36	100.46
(atomic%)			
Cu	22.58	24.23	24.12
Fe	27.78	26.22	26.32
Zn	0.04	0.12	0.00
Co	0.05	—	0.01
S	49.55	49.43	49.55

^a Analysis numbers designate the following samples:

1. One of broad lamellae in isocubanite, 649B-1D-8D, 90–120 cm(b).
2. Large grain in the coarsely crystalline massive sample, 649B-1D-8E, 120–150 cm(c).
3. Discrete grain in the friable sample, 649B-1D-8, 50–56 cm.

Chalcopyrite

The lamellar chalcopyrite in isocubanite from the Snake Pit sulfide deposit deviates significantly from stoichiometry toward more Fe-rich compositions culminating at $\text{Cu}_{22.6}\text{Fe}_{27.8}\text{S}_{49.6}$ (No. 1 in Table 7). Most of the lamellar chalcopyrite compositions are plotted outside of the narrow field defined for the chalcopyrite solid solution at 350°C in the system Cu-Fe-S (Fig. 3).

Discrete grains of chalcopyrite in the yellow massive fragments and friable, unconsolidated material are rich in Fe and also are not strictly stoichiometric in composition. Their composition does, however, fall within the field of the chalcopyrite solid solution at 350°C, suggesting that the discrete chalcopyrite did not co-precipitate with isocubanite. The Zn and Co contents of the lamellar chalcopyrites are generally very low, compared with those of the associated isocubanite, although some of the chalcopyrite contains appreciable amounts of Zn (e.g., No. 2 in Table 7).

Compositional variations similar to the Snake Pit chalcopyrite are reported for those from the EPR 21°N deposit (Lafitte et al., 1985). These authors have also recognized that the chalcopyrite in association with cubanite (isocubanite) is richer in Fe than that not associated with cubanite.

Sphalerite

Sphalerite from the Snake Pit massive sulfide specimens was classified into three groups: (1) associated with isocubanite, (2) associated with chalcopyrite, and (3) constituting a colloform structure with marcasite (or pyrite). All three groups are observed in the friable, unconsolidated material. Back-scattered electron images show that the colloform sphalerites are characterized by very finely banded or concentrically zoned structures (Plate 2-6). Some of the colloform sphalerite is so finely banded that it was only possible to obtain average compositions of several compositionally different bands by microprobe analyses. The concentrically zoned colloform sphalerite commonly has domains that show different brightness in the back-scattered electron images. Also, sector-zoned sphalerite from the gray massive fragments has domains with different brightness in the back-

scattered electron images. Microprobe analyses were carried out on several such domains (Fig. 4 and Table 8).

The FeS contents for different domains of the sector-zoned sphalerite and the concentrically zoned colloform sphalerite are extremely variable; e.g., 23.5 to 38.5 mole% for a single, sector-zoned sphalerite grain and from 10.2 to 19.6 mole% for a concentrically zoned colloform sphalerite grain (Table 8). Although such large variations in the FeS contents are usual for a single sphalerite grain, it is clear from Figure 4 that the highest FeS contents in sphalerite are associated with isocubanite, the lowest FeS contents with the colloform structures, and intermediate FeS contents with chalcopyrite. The CdS contents of the colloform sphalerite are significantly lower than those of sphalerite coexisting with isocubanite and chalcopyrite (Fig. 4). MnS contents are very low (<0.2 wt%) in all the three groups of sphalerite.

Wide compositional variations in sphalerite and wurtzite are also recognized in the sulfide deposits from the EPR at 21°N (Styrt et al., 1981; Zierenberg et al., 1984; Lafitte et al., 1985), and from the Juan de Fuca Ridge (Koski et al., 1984; Tivey and Delaney, 1986; Davis et al., 1987). Like the colloform sphalerite from the Snake Pit deposit, those from the Juan de Fuca Ridge tend to have relatively low FeS contents (3.6 to 9.8 mole%) when compared with the overall range (2.0 to 32.3 mole%) observed in other types of sphalerite (Koski et al., 1984).

Pyrrhotite

The compositional range for pyrrhotite is very limited (i.e., 46.6 to 47.2 atomic% total metals; Table 9). Trace amounts of Co range from 0.02 to 0.27 atomic%. The Co/Fe atomic ratios of pyrrhotite are nearly the same as for the isocubanite with which it is associated. Trace amounts of Cu up to 0.17 atomic% were detected in pyrrhotite enclosed by isocubanite (Table 9). The highest concentration of Cu (0.17 atomic%) in this pyrrhotite is close to the experimentally-determined maximum concentration of Cu in pyrrhotite in equilibrium with isocubanite, pyrite, and chalcopyrite at 350°C (Hutchison and Scott, 1981).

A composition of the gray alteration mineral derived from pyrrhotite is listed in Table 9 (No. 4). An alteration mineral similar to this gray mineral occurs in the sulfide deposit at the EPR 21°N (Hekinian et al., 1980).

DISCUSSION

Source of sulfur

The hydrothermal solutions that yield submarine sulfide deposits are derived largely from the seawater that circulates through cracks and fissures of the hot oceanic crust and leached sulfide sulfur and metals (e.g., Hekinian et al., 1980; Styrt et al., 1981). Pyrrhotite occurs as a primary sulfide in almost all the Snake Pit sulfide specimens, indicating that the hydrothermal solutions responsible for the major sulfide minerals were strongly reducing. In such solutions, sulfate cannot be present in equilibrium with sulfide species. Therefore, we can reasonably assume that any incorporated seawater sulfate in the hydrothermal solutions was completely reduced to sulfide in the present case. It is likely that the somewhat low $\delta^{34}\text{S}$ values for the Snake Pit sulfide specimens compared to the eastern Pacific sulfide samples reflect the smaller contribution of seawater sulfate.

Mineral deposition, exsolution, and alteration

The high-temperature assemblage isocubanite (iss) + pyrite gives way to the low-temperature assemblage chalcopyrite + pyrrhotite below 334°C (Yund and Kullerud, 1966). Therefore,

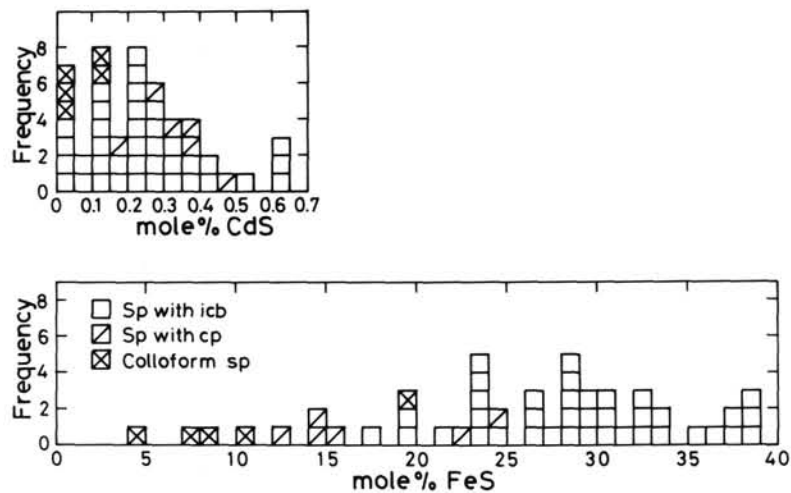


Figure 4. Frequency distribution of FeS and CdS contents in sphalerites. Open squares indicate the sphalerites associated with isocubanite; open squares with an oblique line indicate those with chalcopyrite; and open squares with a cross indicate colloform sphalerites with or without marcasite.

Table 8. Representative microprobe analyses of sphalerite.

Analysis no. ^a	1	2	3	4	5	6	7	8
(wt%)								
Zn	41.31	51.12	49.44	49.07	56.32	62.27	54.58	60.05
Fe	23.06	13.51	15.90	16.22	9.17	2.52	11.44	5.10
Cu	0.64	0.96	1.03	0.55	0.44	0.00	0.40	0.47
Co	0.08	0.04	0.11	0.01	0.20	0.00	n.d.	n.d.
Mn	0.01	0.02	0.02	0.03	0.01	0.01	0.00	0.00
Cd	0.38	0.51	0.34	0.30	0.55	0.10	0.17	0.00
S	33.91	33.23	33.62	33.74	33.10	32.80	33.21	33.03
Total	99.39	99.39	100.46	99.92	99.79	97.70	99.80	98.65
(atomic%)								
Zn	29.87	37.60	35.85	35.68	41.57	47.14	40.10	44.89
Fe	19.49	11.62	13.48	13.79	7.92	2.23	9.83	4.46
Cu	0.48	0.72	0.76	0.41	0.33	0.00	0.31	0.36
Co	0.06	0.03	0.09	0.00	0.16	0.00	-	-
Mn	0.01	0.02	0.02	0.03	0.01	0.01	0.00	0.00
Cd	0.16	0.22	0.14	0.12	0.24	0.05	0.07	0.00
S	49.93	49.79	49.66	49.97	49.77	50.57	46.69	50.29

^a Analysis numbers designate the following samples:

1. Dark domain in the back-scattered electron image, sector-zoned sphalerite with growth bands of isocubanite, 649B-1D-7, 84–90 cm.
2. Light-gray domain in the back-scattered electron image, the same grain as Analysis 1.
3. Sphalerite with isocubanite blebs and enclosed in isocubanite from the massive sample with euhedral pyrite, 649G-1D-1, 2 cm.
4. Associated with isocubanite grains having abundant chalcopyrite lamellae, 649B-1D-8E, 120–150 cm(b).
5. From the yellow massive fragment, 649B-1D-8E, 120–150 cm(c).
6. Colloform sphalerite with the least Fe content, 649B-1D-8, 50–56 cm.
7. Sphalerite analysis with the maximum Fe content obtained for a strongly zoned grain of colloform sphalerite, 649B-1D-8E, 120–150 cm(e).
8. Sphalerite analysis with the minimum Fe content obtained for the same sphalerite grain as Analysis 7.

the equilibrium association of isocubanite with pyrite provides us with a solid criterion for limiting the temperature conditions under which these minerals precipitate. In the Snake Pit massive sulfides, euhedral pyrite grains occur sparsely together with spherical isocubanite rimmed by chalcopyrite and with interstitial pyrrhotite. The coexisting sphalerite, however, contains 25–29 mole% FeS (e.g., No. 3 in Table 8), indicating that the sulfur fugacity (f_{S_2}) at which the Snake Pit isocubanite precip-

itated was lower than that of pyrite-pyrrhotite equilibrium (Barton and Toulmin, 1966). It follows that the euhedral pyrite might have precipitated later than isocubanite, as in the case of anhedral pyrite and marcasite. The temperature of hydrothermal solution measured directly by the submersible *Alvin* is higher than that of the pertinent tie line change in the system Cu-Fe-S, but this measured temperature is not substantiated by the mineral assemblages of the Leg 106 Snake Pit specimens.

Table 9. Microprobe analyses of pyrrhotite and its alteration product.

Analysis no. ^a	1	2	3	4
(wt%)				
Fe	59.61	60.96	60.61	39.76
Cu	n.d.	n.d.	0.25	4.65
Co	0.37	0.22	0.03	0.01
S	39.53	39.35	39.57	28.28
Total	99.51	100.53	100.46	72.70
(atomic%)				
Fe	46.28	47.00	46.70	42.70
Cu	—	—	0.17	4.39
Co	0.27	0.16	0.02	0.01
S	53.45	52.84	53.11	52.90

^a Analysis numbers designate the following samples:

1. Pyrrhotite, 649B-1D-8, 50–56 cm.
2. Pyrrhotite, 649B-1D-8E, 120–150 cm(b).
3. Pyrrhotite, 649B-1D-8D, 90–120 cm(a).
4. Alteration phase derived from pyrrhotite, 649B-1D-8D, 90–120 cm(a).

The precipitation of discrete chalcopyrite grains probably occurred under the f_{S_2} -T conditions somewhat different from those under which isocubanite was formed; this is based on the following observations: (1) the amounts of sphalerite as well as its FeS contents are very different between the isocubanite-dominant and chalcopyrite-dominant massive sulfide specimens, and (2) discrete grains of isocubanite and chalcopyrite do not coexist with each other. The colloform marcasite-sphalerite may have precipitated under the f_{S_2} -T conditions different from those under which the above two minerals precipitated.

The primary Fe-rich isocubanite of the first group, that precipitated with pyrrhotite, had exsolved small amounts of chalcopyrite probably due to falling temperature, and then was quenched when trace amounts of pyrrhotite started to form as exsolution lamellae. It seems likely, therefore, that the most Fe-rich isocubanite ($Cu_{14.9}Fe_{35.4}Zn_{0.1}S_{49.6}$) should be close in composition to the Fe-rich extremities of isocubanite. According to the hydrothermal experiments carried out between 300° and 500°C and a pressure of 500 kg/cm² in the system Cu-Fe-Zn-S (Kojima and Sugaki, 1985), the Fe content of iss increases with decreasing temperature, reaching the composition $Cu_{14.9}Fe_{35.2}Zn_{0.7}S_{49.2}$ at 300°C which, except for the Zn content, is very close to the composition of the most Fe-rich isocubanite from Snake Pit. It is likely that the increase of Fe in isocubanite ceased at about 300°C, and with further decrease in temperature and the resultant exsolution of pyrrhotite, the trend in the compositional change of isocubanite reversed toward stoichiometric cubanite. The other groups of Snake Pit isocubanite might have been quenched before the onset of pyrrhotite exsolution. Some isocubanite grains were quenched without displaying any sign of exsolution, especially in the friable, unconsolidated material. Such grains must have undergone a cooling history different from that experienced by the massive sulfide. They generally have spherical forms without clastic textures and they could be rapidly cooled fallouts of particulates emitted from the black smoker vents. The coarsely crystalline massive fragments and the gray fragments with sphalerite band may be chimney debris. The brassy yellow fragments composed of spherical isocubanite grains are of uncertain origin.

Metasomatic sulfidation changes isocubanite to chalcopyrite with or rarely without Fe-disulfide phases. The textural

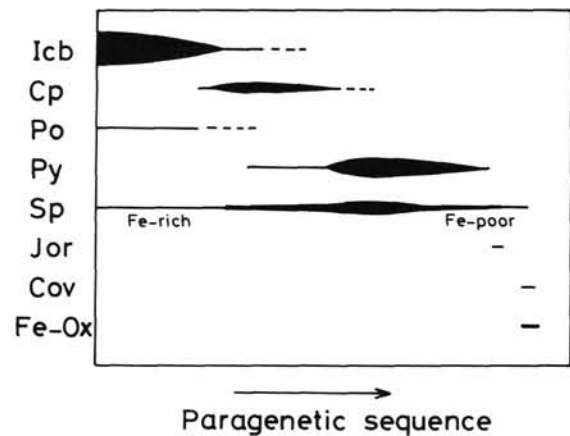


Figure 5. Paragenetic sequence of minerals for the Snake Pit hydrothermal deposit. Abbreviations for minerals are the same as in Table 1, except for py which indicates both pyrite and marcasite.

evidence for such reaction is seen in the spherical isocubanite grains with a chalcopyrite rim. Some grains are almost completely converted to chalcopyrite with only traces of isocubanite remaining in the core. The metasomatic mineral changes might have occurred under low temperature conditions in the Snake Pit sulfide mound. If this is the case, the assemblage chalcopyrite + isocubanite + Fe-disulfides may represent a metastable transition toward the assemblage pyrite + chalcopyrite.

No isocubanite-bearing assemblages have been so far described in on-land sulfide deposits, nor has cubanite deviating extremely from stoichiometric composition. This is probably because isocubanite initially deposited on the seafloor has undergone various compositional and phase changes during the subsequent deep burial and uplift. Exsolution of chalcopyrite and pyrrhotite may very much diminish the amounts of isocubanite present initially, particularly when isocubanite is initially Cu-rich. The remaining isocubanite would be converted to orthorhombic cubanite at about 200°–210°C if the f_{S_2} was maintained low enough for pyrite to be unstable (Cabri, 1973). Also, isocubanite easily breaks down to chalcopyrite with or without pyrite, particularly when f_{S_2} is high enough for pyrite to be stable. The persistence of isocubanite at the Snake Pit sulfide deposit, however, indicates that rapid cooling coupled with effective sealing from subsequent mineral changes can preserve isocubanite.

The mineralogical features outlined above for the Snake Pit sulfides are consistent with the following model of mineral deposition. The high temperature solutions emitted from the black smoker vents have low f_{S_2} and low f_{O_2} values, and isocubanite precipitates together with small amounts of pyrrhotite right around the active vents. Probably due to increasing degree of mixing with the ambient cold seawater, the temperature of solutions decreases whereas the f_{S_2} and f_{O_2} increase away from the vents, which causes the successive precipitation of chalcopyrite plus sphalerite and then colloform sphalerite-pyrite. During the continued, subsequent mineralization, fallout of particulates and chimney debris suffered sulfidation and oxidation. Certainly, some modifications are necessary for this simple model in order to explain all the details of mineral textures such as the zoned grains composed of chalcopyrite, isocubanite, and sphalerite in this sequence from the core to rim. Figure 5 schematically depicts the paragenetic sequence of mineral formation.

CONCLUSIONS

1. The average composition obtained from five bulk sample analyses of the friable, unconsolidated material indicates that it is characterized by high Cu/Zn ratio, high Cu and Co contents, and low Pb and Ag contents.

2. Isocubanite is one of the most abundant phases in the Snake Pit sulfide specimens. It contains considerable amounts of Co, which is responsible for the high Co contents observed in bulk analyses of the Snake Pit sulfide specimens.

3. The Snake Pit isocubanite almost invariably has chalcopyrite exsolution lamellae, and occasionally exsolution bodies of pyrrhotite. The isocubanite became Fe-rich as chalcopyrite continued to exsolve, and then its compositional trend reversed toward stoichiometric cubanite at the onset of pyrrhotite exsolution. The isocubanite that contains exsolved pyrrhotite is generally rich in Fe with the most Fe-rich composition being $\text{Cu}_{14.9}\text{Fe}_{35.4}\text{Zn}_{0.1}\text{S}_{49.6}$.

4. Spherical isocubanite grains without exsolution phases occur in the friable, unconsolidated material. It is likely that these isocubanite grains are rapidly cooled fallout emitted from black smokers.

5. The FeS contents of the Snake Pit sphalerite are very variable. The highest FeS contents of the Snake Pit sphalerite are observed in association with isocubanite, intermediate FeS contents in association with discrete grains of chalcopyrite, and the lowest FeS contents in association with colloform marcasite (or pyrite). This result suggests that isocubanite, discrete chalcopyrite, and colloform marcasite precipitated under different condition, probably different temperatures.

6. Low temperature sulfidation converts isocubanite to the assemblage chalcopyrite + pyrite. The assemblage isocubanite + pyrite + chalcopyrite observed in the Snake Pit specimens probably represents a transitional stage toward the assemblage pyrite + chalcopyrite.

7. Sulfur isotope ratios of the Snake Pit sulfide specimens are very uniform, ranging from +1.2 to +2.8‰. These values are apparently low compared to those of the sulfide samples from the eastern Pacific deposits. This suggests smaller contribution from reduced seawater sulfate in the Snake Pit sulfide deposit.

ACKNOWLEDGMENTS

We thank M. Kusakabe of the Institute for Study of the Earth's Interior of Okayama University for use of mass spectrometry facilities. T. Saito provided valuable technical assistance. We also thank J. Honnorez and two anonymous reviewers for their thorough reviews and helpful comments which led to the substantial improvement of the manuscript.

REFERENCES

Ariyoshi, H., Kimura, M., and Toei, K., 1960. UV spectrophotometric determination of trace amounts of selenium with o-phenylenediamine. *Talanta*, 5:112-118.

Arnold, M., and Sheppard, S.M.F., 1981. East Pacific Rise at latitude 21°N: isotopic composition and origin of the hydrothermal sulfur. *Earth Planet. Sci. Lett.*, 56:148-156.

Barton, P. B., Jr., and Toulmin, P., III., 1966. Phase relations involving sphalerite in the Fe-Zn-S system. *Econ. Geol.*, 61:815-849.

Bischoff, J. L., Rosenbauer, R. J., Aruscavage, P. J., Baedecker, P. A., and Crock, J. G., 1983. Sea-floor massive sulfide deposits from 21°N, East Pacific Rise; Juan de Fuca Ridge; and Galapagos Rift: Bulk chemical composition and economic implications. *Econ. Geol.*, 78:1711-1720.

Cabri, L. J., 1973. New data on phase relations in the Cu-Fe-S system. *Econ. Geol.*, 68:443-454.

Caye, R., Cervelle, B., Cesbron, F., Oudin, E., Picot, P., and Pillard, F., 1988. Isocubanite, a new definition of the cubic polymorph of cubanite CuFe_2S_3 . *Mineral. Mag.*, 52:509-514.

Davis, E. E., Goodfellow, W. D., Bornhold, B. D., Adshead, J., Blaise, B., Villinger, H., and Le Cheminant, G. M., 1987. Massive sulfides in a sedimented rift valley, northern Juan de Fuca Ridge. *Earth Planet. Sci. Lett.*, 82:49-61.

Detrick, R. S., Honnorez, J., Adamson, A. C., Brass, G., Gillis, K. M., Humphris, S. E., Mevel, C., Meyer, P., Petersen, N., Rautenschlein, M., Shibata, T., Staudigel, H., Yamamoto, K., and Woodridge, A.L., 1986. Drilling the Snake Pit hydrothermal sulfide deposit on the Mid-Atlantic Ridge, lat 23°22'N. *Geology*, 14:1004-1007.

Hannington, M. D., Peter, J. M., and Scott, S. D., 1986. Gold in sea-floor polymetallic sulfide deposits. *Econ. Geol.*, 81:1867-1883.

Hekinian, R., Fevrier, H., Bischoff, J. L., Picot, P., and Shanks, W. C., 1980. Sulfide deposits from the East Pacific Rise near 21°N. *Science*, 207:1433-1444.

Hutchison, M. H., and Scott, S. D., 1981. Sphalerite geobarometry in the Cu-Fe-Zn-S system. *Econ. Geol.*, 76:143-153.

Kerridge, J. F., Haymon, R. M., and Kastner, M., 1983. Sulfur isotope systematics at the 21°N site, East Pacific Rise. *Earth Planet. Sci. Lett.*, 66:91-100.

Kojima, S., and Sugaki, A., 1985. Phase relations in the Cu-Fe-Zn-S system between 500°C and 300°C under hydrothermal conditions. *Econ. Geol.*, 80:158-171.

Koski, R. A., Clague, D. A., and Oudin, E., 1984. Mineralogy and chemistry of massive sulfide deposits from the Juan de Fuca Ridge. *Geol. Soc. Am. Bull.*, 95:930-945.

Pockalny, R. A., Detrick, R. S., and Fox, P. J., 1985. SeaBeam map of the Kane transform: Implications for the tectonics of slow-slipping transform faults. *EOS*, 66:1092.

Lafitte, M., Maury, R., Perseil, E. A., and Bouleque, J., 1985. Morphological and analytical study of hydrothermal sulfides from 21° north East Pacific Rise. *Earth Planet. Sci. Lett.*, 73:53-64.

Shanks, W. C., III., and Seyfried, W. E., 1987. Stable isotope studies of vent fluids and chimney minerals, Southern Juan de Fuca Ridge: Sodium metasomatism and seawater sulfate reduction. *J. Geophys. Res.*, 92:11387-11399.

Shanks, W. C., III., Koski, R. A., and Woodruff, L. G., 1984. Mineralogy and stable isotope systematics of sulfide deposits from the Juan de Fuca Ridge. *EOS*, 65:1113.

Skirrow, R., and Coleman, M. L., 1982. Origin of sulfur and geothermometry of hydrothermal sulfides from the Galapagos Rift, 86°N. *Nature*, 299:142-144.

Styrt, M. M., Brackmann, A. J., Holland, H. D., Clark, B. C., Pisutha-Arnold, V., Eldridge, C. S., and Ohmoto, H., 1981. The mineralogy and the isotopic composition of sulfur in hydrothermal sulfide/sulfate deposits on the East Pacific Rise, 21°N latitude. *Earth Planet. Sci. Lett.*, 53:382-390.

Sugaki, A., Shima, H., Kitakaze, A., and Harada, H., 1975. Isothermal phase relations in the system Cu-Fe-S under hydrothermal conditions at 350°C and 300°C. *Econ. Geol.*, 70:806-823.

Sulanowska, M., Humphris, S. E., Thompson, G., and Schroeder, B., 1986. Hydrothermal mineralization in the MARK area, Mid-Atlantic Ridge 23°N. *EOS*, 67:1214.

Sweatman, T. R., and Long, J.V.P., 1969. Quantitative electron-probe microanalysis of rock-forming minerals. *J. Petrol.*, 10:332-379.

Tivey, M. K., and Delaney, J. R., 1986. Growth of large sulfide structures on the Endeavour segment of the Juan de Fuca Ridge. *Earth Planet. Sci. Lett.*, 77:303-317.

Yanagisawa, F., and Sakai, H., 1983. Thermal decomposition of barium sulfate-vanadium pentoxide-silica glass mixtures for preparation of sulfur dioxide in sulfur isotope ratio measurements. *Anal. Chem.*, 55:985-987.

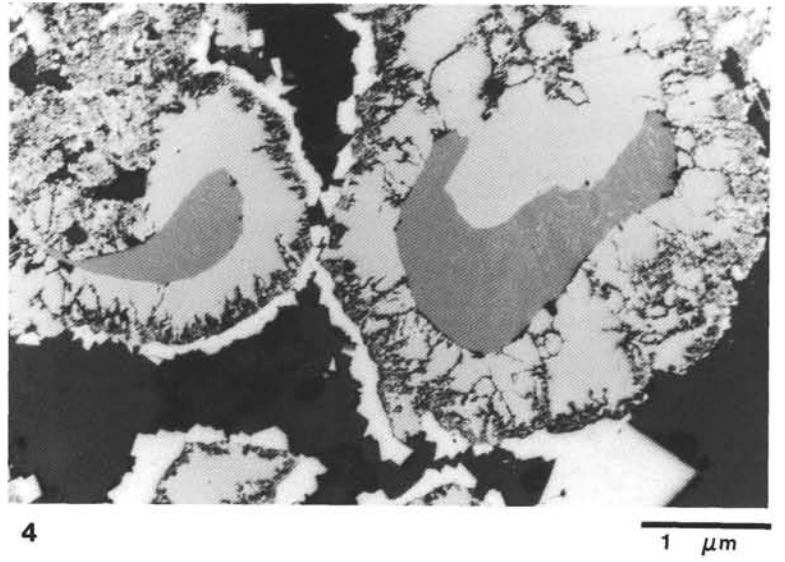
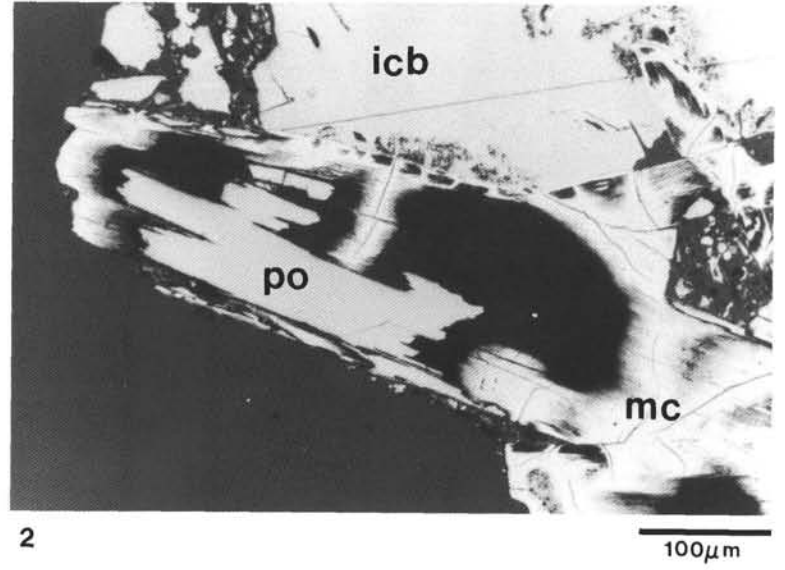
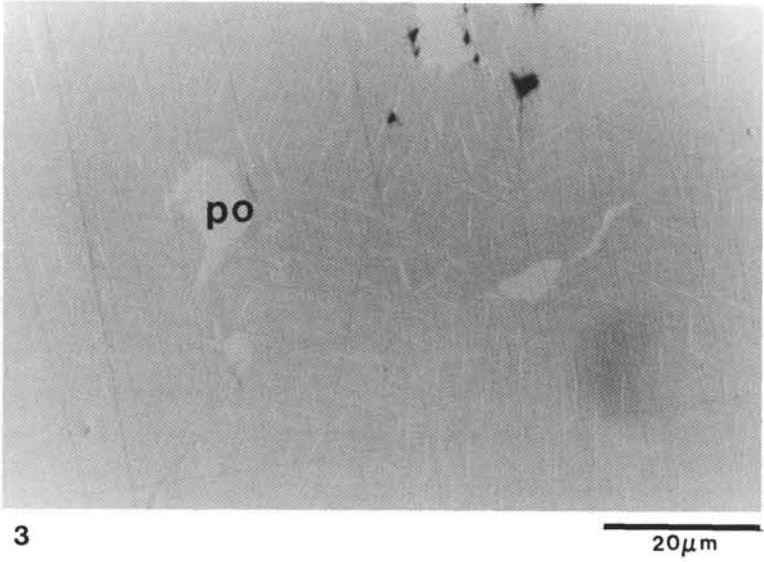
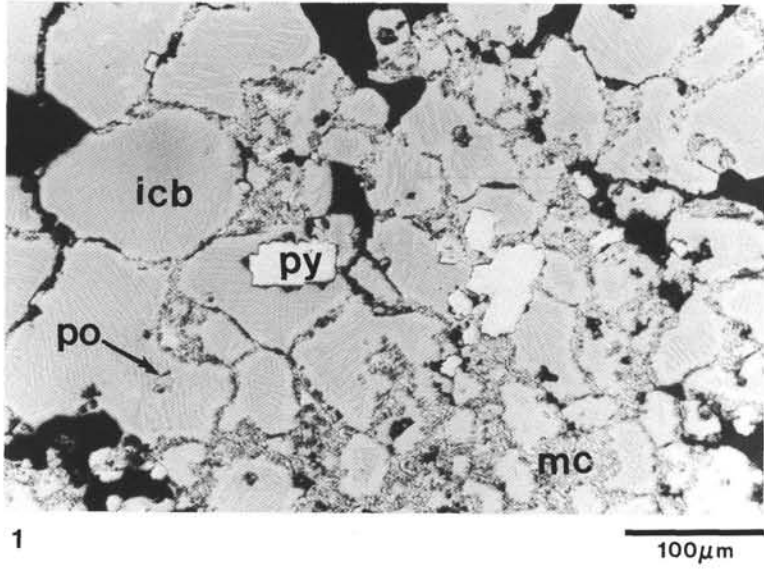
Yund, R. A., and Kullerud, G., 1966. Thermal stability of assemblages in the Cu-Fe-S system. *J. Petrol.*, 7:454-488.

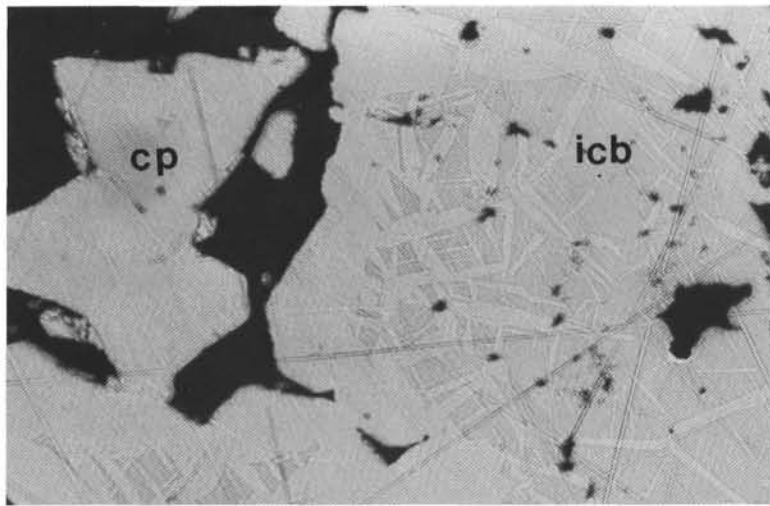
Zierenberg, R. A., Shanks, W. C., III., and Bischoff, J. L., 1984. Massive sulfide deposits at 21°N, East Pacific Rise: chemical composition, stable isotopes, and phase equilibria. *Geol. Soc. Am. Bull.*, 95:922-929.

Date of initial receipt: 21 January 1988

Date of acceptance: 30 May 1989

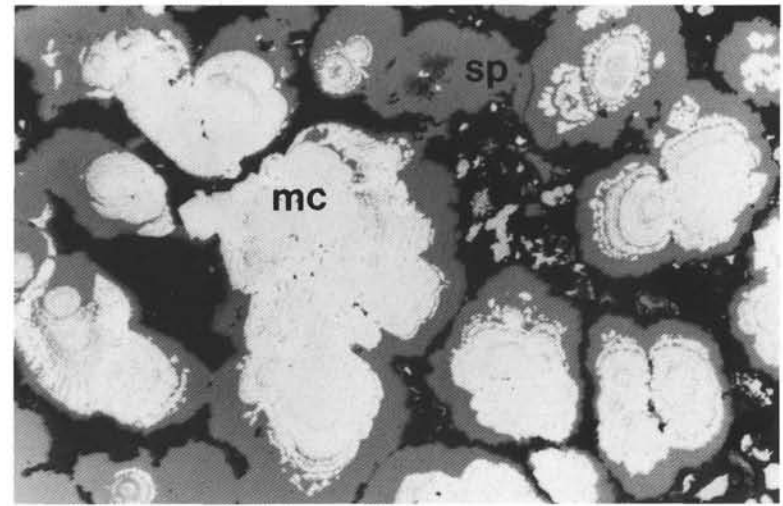
Ms 106/109B-139





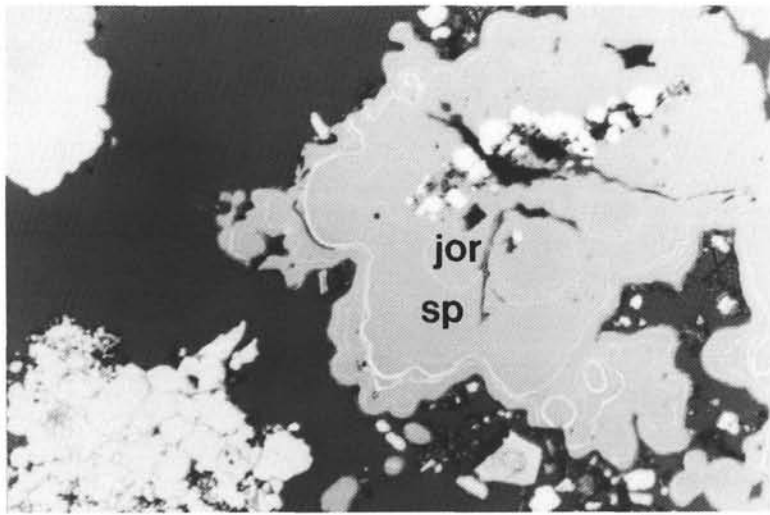
5

100μm



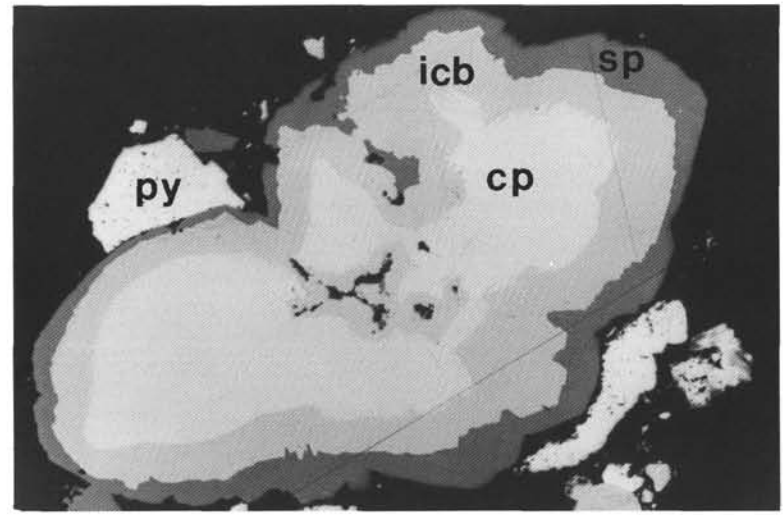
6

100μm



7

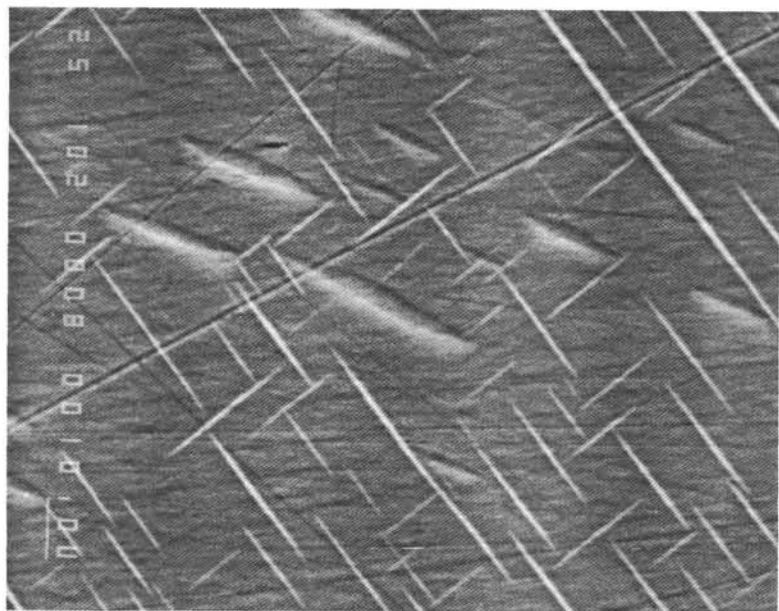
100μm



8

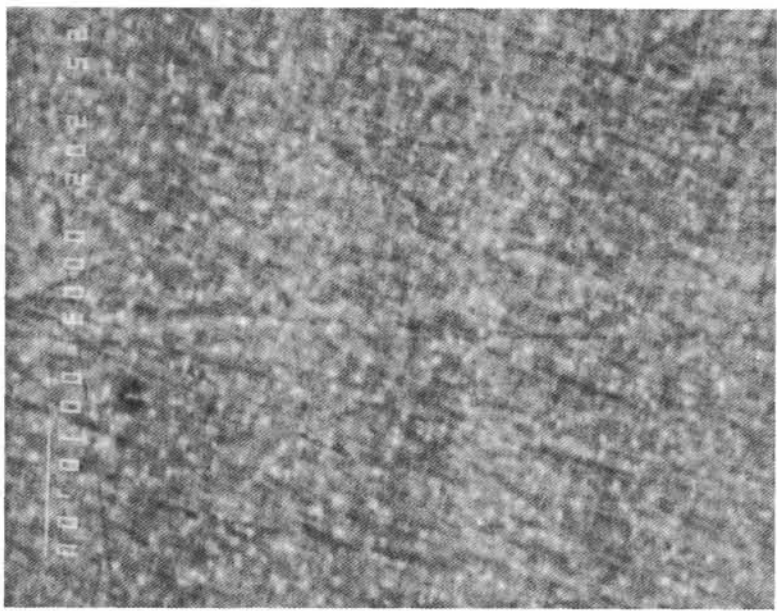
100μm

Plate 1. Photomicrographs in reflected light of the Snake Pit sulfide samples. 1. Sample 649G-1D-1, 2 cm. Aggregates of spherical isocubanite grains with chalcopyrite exsolution lamellae and a chalcopyrite rim. Euhedral pyrite grains are partially enclosed in isocubanite grains. Granular and short prismatic pyrrhotites commonly occur in the cores of isocubanite grains. Also note that tiny grains of marcasite and chalcopyrite occur along the boundaries of adjoining isocubanite grains. 2. Sample 649B-1D-8, 50–56 cm. Long prismatic pyrrhotite. The mineral is partially replaced by marcasite. 3. Sample 649B-1D-8D, 90–120 cm. Exsolution bodies of pyrrhotite in isocubanite grains with small amounts of chalcopyrite lamellae. 4. Sample 649G-1D-1, 2 cm. Sphalerite enclosed in isocubanite with shrinkage cracks. This isocubanite is in turn surrounded by pyrite. Note isocubanite blebs in the sphalerite. 5. Sample 649B-1D-8D, 90–120 cm. The isocubanite-rich and chalcopyrite-rich portions of a yellow massive sulfide fragment. Small amounts of isocubanite remain at the central parts of the chalcopyrite grains in the chalcopyrite-rich portion of the specimen. 6. Sample 649B-1D-8, 50–56 cm. Colloform marcasite with a sphalerite overgrowth. 7. Sample 649B-1D-8, 50–56 cm. Jordanite-like mineral occurring as thin growth bands in colloform sphalerite. 8. Sample 649B-1D-8, 50–56 cm. The composite grain zoned concentrically from chalcopyrite at the core through isocubanite to sphalerite at the rim. Abbreviations for minerals are as follows: icb = isocubanite; py = pyrite; mc = marcasite; po = pyrrhotite; sp = sphalerite; cp = chalcopyrite; and jor = jordanite.



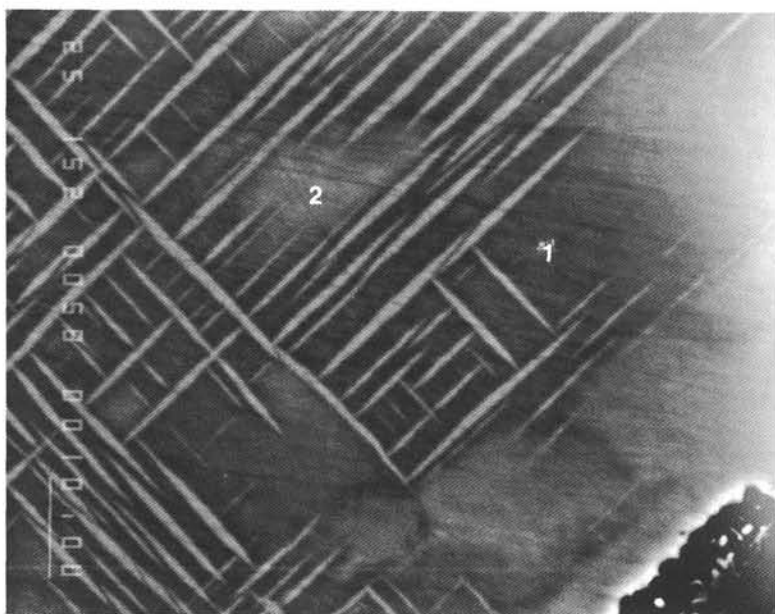
2

10μm



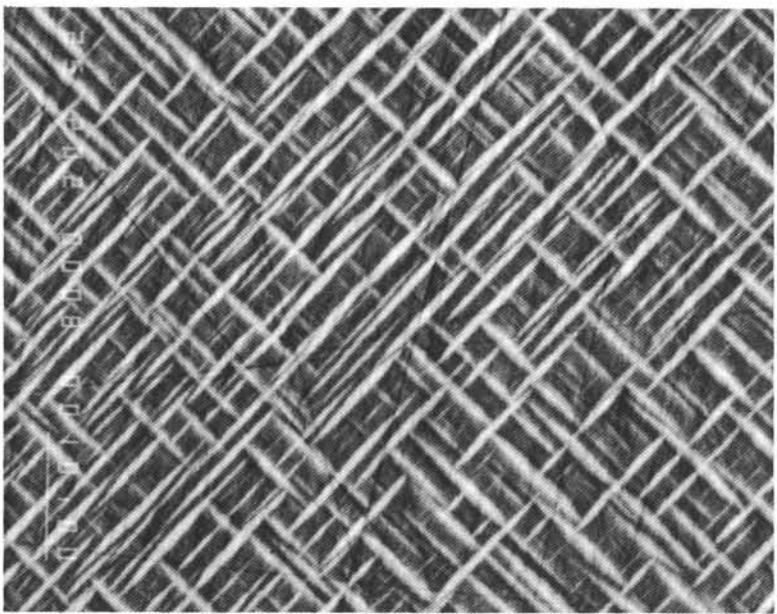
1

10μm



4

10μm



3

10μm

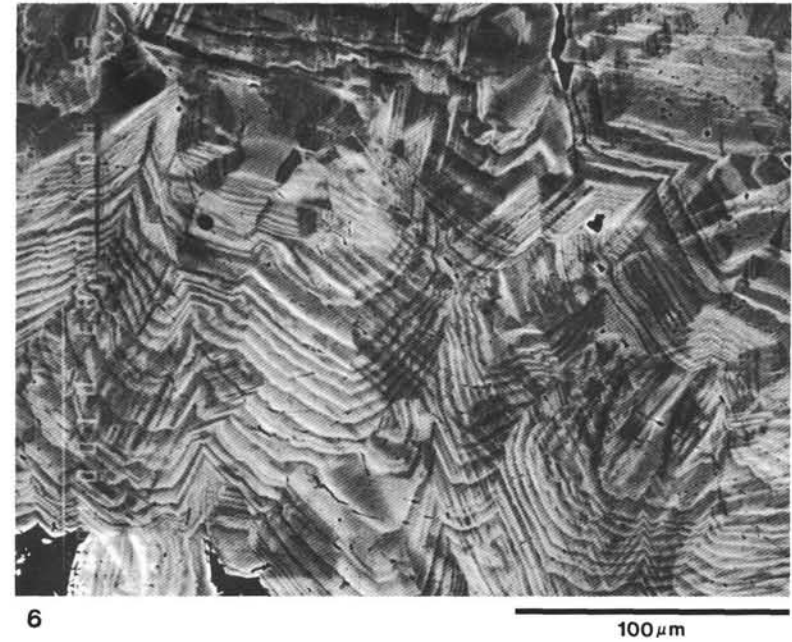
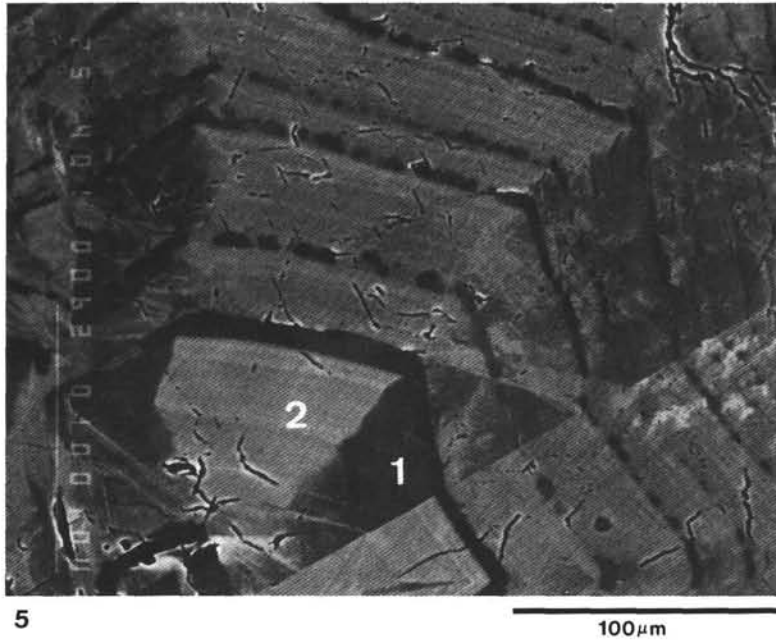


Plate 2. Back-scattered electron photomicrographs of polished specimens of the Snake Pit sulfide minerals. 1. Sample 649G-1D-1, 2 cm. Isocubanite mottled with abundantly distributed, exsolution bodies (bright spots). 2. Sample 649B-1D-8D, 90–120 cm. Isocubanite with rectangular, lattice-like exsolution lamellae of chalcopyrite. Another unidentified phase exsolves diagonally to the rectangular chalcopyrite lamellae. 3. Sample 649B-1D-8E, 120–150 cm. Isocubanite with dense chalcopyrite lamellae. 4. Sample 649G-1D-1, 14–16 cm, #4. Isocubanite having domains with different compositions. The bright domain (2) is rich in Cu, and the dark domain (1) is rich in Fe. The bright area on the right side of the photo is due to halation from presence of amorphous silica. 5. Sample 649B-1D-7, 84–90 cm. Sector-zoned sphalearite. Numbers 1 and 2 indicate points at which sphalearite analyses 1 and 2, respectively, in Table 8 were obtained. 6. Sample 649B-1D-7, 84–90 cm. Colloform sphalearite with dense, thin growth bands.